APCC
APEC CLIMATE CENTER

TECHNICAL REPORT

APCC
APEC CLIMATE CENTER

PREFACE

It is our pleasure to present to you the APEC Climate Center (APCC)'s Technical Report 2012, which reports the core outcomes of our research activities from the past year.

Since 2005, APCC, as a hub of climate information in the Asia-Pacific region, has strived to share our analysis and prediction of abnormal climate and to apply this information to regional development. The Center has established the most extensive Multi-Model Ensemble (MME) system for seasonal prediction in the world through its international science network and has provided value-added products to various stakeholders. Recently, APCC has expanded its mandate to include enhancing the capacity of APEC member economies to respond effectively to climate change and variability through better application of climate information.

In 2012, APCC continued to make an effort to improve the quality and quantity of our short-term climate forecasts and our online climate information systems, as information dissemination tools. Additionally, APCC began its endeavor to produce more applicable climate information through interdisciplinary research among various sectors, such as agriculture and hydrology. The following technical report provides more information about our research outcomes from 2012.

In 2013, following APCC's goal to enhance socioeconomic well-being through better utilization of climate information, APCC will continue to improve the quality and accuracy of its climate information, recognizing that the utility of this information is only as good as its quality. We would like to make the best use of our research outcomes in various scientific and application areas. We welcome any feedback on this report or on our services.

My best and warmest regards to all of you.

Dr. Chin-Seung Chung
Director/APEC Climate Center

CONTENTS

APCC

TECHNICAL REPORT 2012-02

Evaluation of Water Balance on a Regional Scale Considering Different Irrigation Systems

Dr. Jong Ahn Chun

ABSTRACT

Food security can be improved through increasing the areas of agricultural land or by implementing more intensive agricultural management, including irrigation practices. The objectives of this study were to incorporate practical irrigation schemes into the NASA Land Information System (LIS) and to use it to investigate the impacts of irrigation schemes on land surface states and fluxes, including evapotranspiration, soil moisture, and runoff, in the Murray-Darling basin, Australia, and in East Asia and the Korean Peninsula. For investigations this year, the Noah-LSM (Noah 3.2-Land Surface Model) in the LIS was selected, to incorporate three different irrigation schemes such as non-irrigation, flood irrigation, drip irrigation, and sprinkler irrigation schemes. These three irrigation schemes were applied in the Murray-Darling basin. However, drip irrigation and sprinkler irrigation schemes were not applied to East Asia and the Korean Peninsula regions, since these schemes are not commonly used in these areas. The Moderate Resolution Imaging Spectrometer (MODIS) vegetation index was used to estimate crop-growing seasons for application in a global experiment. The flood irrigation scheme increased the latent heat flux (QLE) and ground heat flux (QG), but decreased the sensible heat flux (QH). In regions with the flood irrigation scheme, evapotranspiration showed a tendency to increase over the growing season. The scheme also increased soil moisture in the first three soil layers (from the surface to 0.6 m deep), while there was no apparent tendency at the fourth soil layer (from 0.6 to 1.0 m deep). Although the impacts of the flood irrigation scheme on the land surface state and fluxes have not been evaluated against observed data in East Asia and the Korean Peninsula, results from the experiments demonstrated that the proposed irrigation scheme can be used to qualitatively investigate impacts on hydrology in these areas.

1. INTRODUCTION

The exchanges of water and energy between the land surface and the atmosphere play a large part in influencing global weather patterns, subsequently affecting communities. The regional climate system and hydrologic cycle can be significantly influenced by agricultural land management, through an alteration of heat and water exchanges between the land and atmosphere (Bonan 1997, 2001; Chase *et al.* 2000). In particular, there have been studies to show agricultural irrigation management affects regional climates and hydrology by modifying the water cycle at or near the land surface (Ben-Gai *et al.*, 2001; Moore and Rojstaczer, 2002; Ozdogan *et al.*, 2006; Lobell and Bonfils, 2008; Lobell *et al.*, 2008).

Water use has increased over the last century. Agricultural uses account for approximately 70% of global freshwater use (Fig. 1), followed by municipal use (approximately 21%). As shown in Fig. 1, the fractions of agricultural water use in developing countries are generally larger than those in developed countries. Agricultural usage in Korea or China accounts for more than 60% of national freshwater use. It is therefore very important for intensive irrigation practices to be accurately investigated in order to estimate land surface states and fluxes in East Asia and the Korean Peninsula. However, irrigation practices have not adequately been represented in estimates of land surface states and fluxes in regional- and global-scale LSMs (Evans and Zaitchik, 2008; Ozdogan *et al.*, 2010).

Land Surface Models (LSMs) have been used to investigate terrestrial water, energy, and biogeochemical processes. The Land Information System (LIS) has been developed to accurately simulate land surface states and fluxes, including soil moisture, evapotranpiration, snow pack, and runoff, by integrating satellite- and ground-based observational datasets with LSMs (Kumar *et al.*, 2006). Studies on the impacts of agricultural water managements on regional climates and hydrology have been conducted using LSMs or Regional Climate Model (RCM) (e.g., Evans and Zaitchik, 2008; Ozdogan *et al.*, 2010. Takat *et al.*, 2003; Sorooshian *et al.*, 2012). Ozdogan *et al.* (2010) suggested that incorporation of irrigation schemes into Numerical Weather Prediction (NWP) models contributes to the potential improvement of weather and climate predictions. Evans and Zaitchik (2008) incorporated various irrigation schemes, including flood- and drip-irrigation, into an LSM and reported that evapotranspiration during irrigation seasons in areas using drip irrigation schemes was reduced by up to 30% compared to traditional irrigation schemes. Haddeland *et al.* (2006) developed an irrigation scheme for the Variable Infiltration Capacity (VIC) LSM and reported that irrigation generally decreased streamflow and increased evapotranspiration in the Colorado and Mekong River basins.

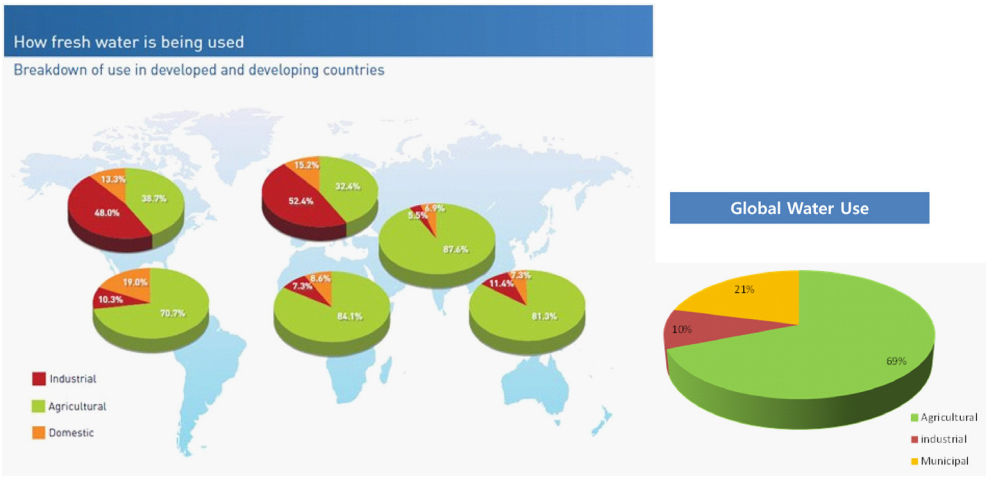

Figure 1 Global freshwater use fractions (adapted from FAO, 2007).

The goals of this study were (1) to incorporate irrigation schemes including flood, drip, and sprinkler irrigations into the NASA Land Information System (LIS), (2) to accurately simulate on-field water consumption on irrigated agricultural land by applying the Noah-LSM (Noah 3.2-Land Surface Model) to the Murray-Darling basin and to East Asia and the Korean Peninsula, and (3) to investigate the impacts of the irrigation schemes on hydrologic flux states, including evapotranspiration, soil moisture, and runoff.

2. METHODOLOGY

2.1 Study site

2.1.1. Murray-Darling Basin, Australia

The Murray-Darling basin (Fig. 2) was selected for this study. The basin consists of the Murray and Darling rivers and their many tributaries (23 river valleys), covering a total area of approximately 1,059,000km^2 (14% of Australia) and has a population of around 2million people. The basin is an important agricultural area because over

one-third of Australia's food supply is typically produced in the region.

The volume of irrigated enterprises in the Murray-Darling basin is the largest in Australia, and the basin produces the highest value in the country (ANRA, n.d.). The basin had a total irrigated area of approximately 1,309,755ha (about 64% of Australia's total area of irrigated crops and pastures) in 1996/97. The irrigation was the dominant water use in the basin, accounting for approximately 95% of the diversion of the basin's water resources. This irrigation accounts for about 75% of the total irrigation in Australia and represents over 50% of all water used in the country.

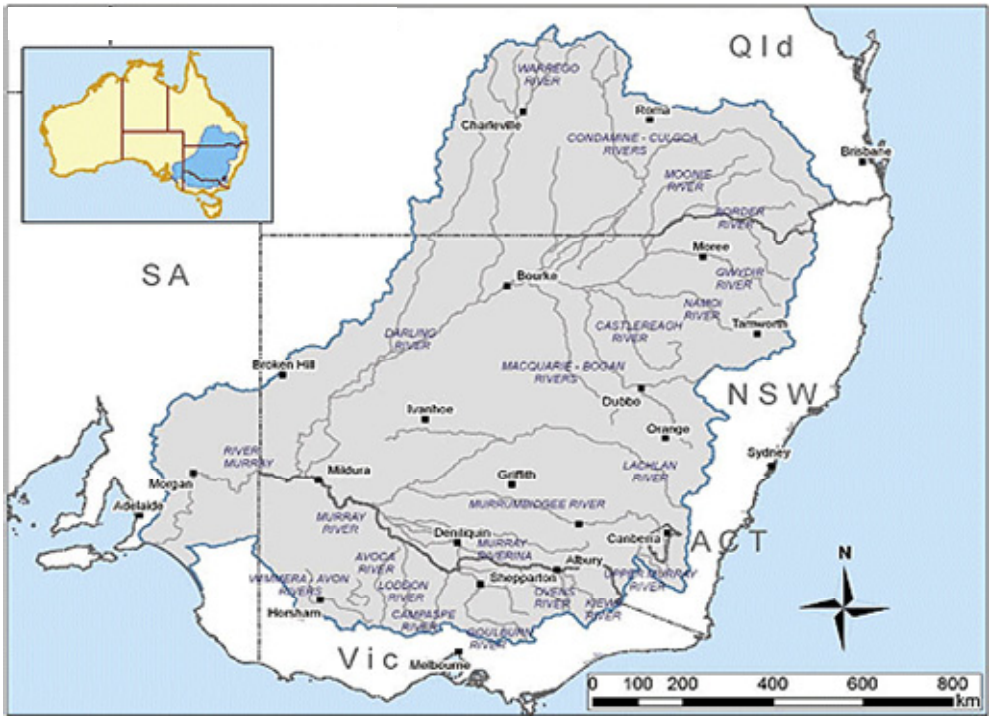

Figure 2 The location map of the Murray-Darling basin (adapted from the Murray-Darling Basin Authority, MDBA, n.d.).

2.1.2. East Asia and the Korean Peninsula

The region of East Asia and the Korean Peninsula (20°N-45°N and 90°E-150°E) was selected for this study (Fig. 3). In this region, agricultural freshwater uses,

including irrigation, account for more than 60% of the total freshwater use in this region. The agricultural use in Japan is approximately 66% of the national freshwater use, that in China accounts for approximately 64%, and that in Korea accounts for approximately 61% of the total of freshwater use for the country.

Figure 3 The study region (East Asia and the Korean Peninsula).

2.2. Data collection

The National Centers for Environmental Prediction Global Data Assimilation System (NCEP GDAS) forcing dataset was used to drive the simulations. The NCEP GDAS data are archived on a 2.5° × 2.5° latitude/longitude grid and are available from the mid 1970s (Abreu *et al.* 2012; Parrish and Derber, 1992). The Tropical Rainfall Measuring Mission (TRMM) was used for supplemental forcing sources. The TRMM meteorological forcing datasets (Huffman *et al.*, 2007) are provided on a global 0.25° × 0.25° grid over the latitude band 50° N-S.

The U.S. Geological Survey (USGS) landcover dataset (USGS, n.d.) was used to identify irrigated areas. The USGS landcover dataset is classified into 24 vegetation types including urban, cropland, deciduous/evergreen forest, and snow or ice. The indices 3 and 4 are irrigated cropland and pasture and mixed dryland/irrigated

cropland and pasture, respectively. For this study, the indices 3 and 4 are assigned to fully saturated irrigation areas and partially (50% of saturation) irrigation areas, respectively.

The United Nations' Food and Agriculture Organization (FAO) soil data were used for sand-, clay-, and silt-fraction maps (Reynolds *et al.* 2000). A global 30 arc-second elevation map (GTOPO30, Gesch *et al.* 1999) was used to derive elevation parameters. GTOPO30 is a global Digital Elevation Model (DEM) with a 30 arc-second spatial resolution (approximately 1 km). The elevation values range from -407 to 8,752 m above mean sea level.

2.3. Noah-LSM

The Land Information System (LIS) has been developed to accurately simulate land surface states and fluxes, including evapotranspiration, soil moisture, snow pack and runoff (Kumar *et al.*, 2006). LIS provides an accurate simulation of land surface states and fluxes through the integration of land surface modeling techniques and satellite- and ground-based observational datasets. As shown in Fig. 3, the system consists of four subsystems: LIS-LSM for land surface modeling, LIS-WRF for coupled land-atmosphere modeling, LIS-DA for data assimilation, and LIS-OPT for advanced optimization and uncertainty modeling.

LIS is a highly modular, flexible, object oriented, and component-based software framework and meets full Earth System Modeling Framework (ESMF) compliance and Assistance for Land Surface Modeling Activities (ALMA) standards (NASA Goddard Space Flight Center, 2010a). The LIS infrastructure can run multiple LSMs for regional domains and the global domain at 1 km to 2.5° spatial resolutions and at temporal resolutions of 15 min to 1 h (NASA Goddard Space Flight Center, 2010b).

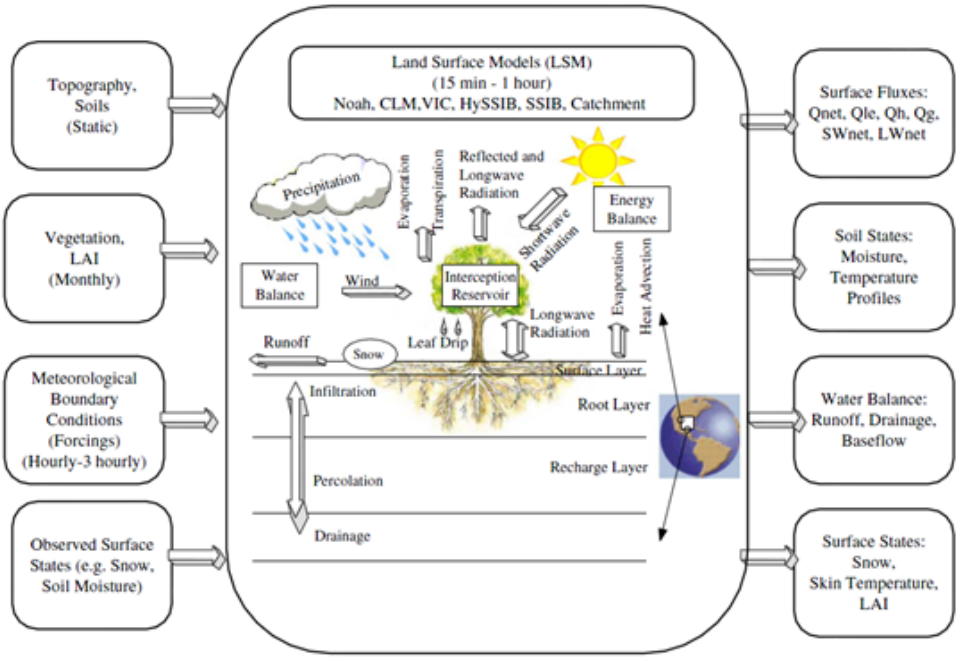

Figure 4 A schematic of the Land Information System (adapted from Kumar *et al.*, 2006).

Noah-LSM has been developed by a number of groups, including NCEP/EMC (NCEP Environmental Modeling Center), OSU (Oregon State University), HRL (NWS Hydrology Lab), AFWA (Air Force Weather Agency), and AFRL (Air Force Research Lab). It is able to simulate land surface states and fluxes, including soil moisture (both liquid and frozen), soil temperature, skin temperature, snowpack depth, snowpack water equivalent, canopy water content, evapotranspiration, and runoff (Koren *et al.*, 1999), and has been operationally used in NCEP models since 1996 (Betts *et al.*, 1997; Ek *et al.*, 2003).

For this study, the Noah-LSM (version 3.2)—a 1-dimensional column model—is used to perform the irrigation experiments. The model can be run in either coupled or uncoupled mode. A Finite Difference Method (FDM) and a Crank-Nicolson Method are implemented to describe the physical processes on the land surface. The Noah-LSM configurations for this study are summarized in Table 1.

Table 1 The LIS configurations for the Noah-LSM.

Parameters or input	values
NOAH32 model output interval	10800 (s)
NOAH32 restart output interval	86400 (s)
NOAH32 soils scheme	1 for Zobler
NOAH32 number of soil layer	4
NOAH32 layer thicknesses	0.1,0.3,0.6, and 1.0 (from surface, m)
NOAH32 initial skin temperature	290 (K)
NOAH32 initial soil temperatures	290, 290, 290, and 290 (K)
NOAH32 initial total soil moistures	0.2, 0.2, 0.2, and 0.2 (m^3 m^{-3})
NOAH32 initial liquid soil moistures	0.2, 0.2, 0.2, and 0.2 (m^3 m^{-3})

2.4. Irrigation schemes

For the global experiment, the irrigation schemes in the LIS were developed to follow growing seasons, using vegetation fractions (VF). The Moderate Resolution Imaging Spectrometer (MODIS) products were used to obtain vegetation fractions to determine crop-growing seasons (details given in Evans and Zaitchik, 2007). The following equation (Eq. [1]) is used to determine growing season thresholds. A growing season will start in the LIS when a vegetation fraction in a grid cell is greater than the growing season threshold value in that grid cell.

$$\text{Growing season threshold} = VF_{min} + 0.4\,(VF_{max} - VF_{min}) \qquad (1)$$

where VF is the vegetation fraction, VFmax is the maximum of VF, and VFmin is the minimum of VF.

2.4.1. Flood irrigation

The flood irrigation scheme will turn on when soil moisture reaches 25% above the wilting point. Irrigation water will be applied until the first soil layer is saturated, where the USGS landcover index is equal 3. Where the USGS landcover index is equal 4, irrigation water will be applied until the soil moisture of the first soil layer

reaches 50%. It was assumed that the irrigation was applied between 0900 and 0930 local time. Since this scheme is the most conventional irrigation method in East Asia and the Korean Peninsula, this scheme was fully simulated for this study.

2.4.2. Drip irrigation

This irrigation scheme is known to be one of the most advanced irrigation practices to save water resources by applying only as much water as is required. It is assumed that the vegetation always has sufficient water to transpire without being stressed and that no excess water is added during the simulation of this scheme. Evapotranspiration (E_t) is affected by the soil moisture in the Noah-LSM through the canopy resistance, R_c (eqs. [2] to [5]).

$$E_t = \sigma_f E_p B_c \left[1 - \sqrt{\frac{W_c}{S}}\right] \quad (2)$$

where

σ_f is the green vegetation fraction.
E_p is the potential evaporation.
B_c is a function of the canopy resistance.
W_c is the intercepted canopy water.
S is the maximum canopy water storage.

A function of the canopy resistance, B_c is given by eq. (3).

$$B_c = \frac{1+\frac{\Delta}{R_r}}{1+R_c C_h+\frac{\Delta}{R_r}} \quad (3)$$

where

C_h is the surface exchange coefficient for heat and moisture.
Δ depends on the slope of the saturation specific humidity curve.
R_r is a function of the surface air temperature, surface pressure and C_h.

$$R_c = \frac{R_{c\,\min}}{\mathrm{LAI} \cdot F_1 \cdot F_2 \cdot F_3 \cdot F_4} \quad (4)$$

where

LAI is the leaf area index.
F_1 is the solar radiation effect (between 0 and 1).
F_2 is the vapor pressure deficit effect (between 0 and 1).
F_3 is the air temperature effect (between 0 and 1).
F_4 is the soil moisture effect (between 0 and 1).

F_4 is given by eq. (5).

$$F_4 = \sum_{i=1}^{3} \frac{(\theta_i - \theta_w) d_{z_i}}{(\theta_{\mathrm{ref}} - \theta_w)(d_{z_1} + d_{z_2} + d_{z_3})} \quad (5)$$

where

i is the soil layer (here 3 soil layers are within the rooting depth).
θ is the fraction of unit soil volume occupied by water.
ref is the reference field capacity soil moisture, which is defined as the minimum soil moisture without soil moisture stress.
w is the wilting point of soil moisture.
d_{zi} is the depth of soil layer i.

2.4.3. Sprinkler irrigation

The root zone was assumed to include the first two soil layers. The irrigation water is applied at a constant rate when the soil moisture of the root zone falls to 10% above the stress point. The sprinkler irrigation will be terminated at 80% of maximum soil moisture. The irrigation rates must be less than the soil infiltration rates to avoid ponding or surface runoff. Appropriate irrigation rates were suggested

as 1 to 20 mm h-1 (Lamaddalena *et al.*, 2007).

3. RESULTS AND DISCUSSION

3.1. Irrigation schemes

Differing irrigation schemes, including flood irrigation, drip irrigation, and sprinkler irrigation, have been incorporated into the LIS in this study so that irrigation type can be selected, and parameters for irrigation schemes and irrigation time can be adjusted in the LIS configuration file. Depending on the irrigation type, additional parameters such as irrigation trigger coefficients for flood and sprinkler irrigation can be adjusted in the configuration file. Configurations for the irrigation experiments are summarized in Table 2.

Table 2 Configurations for the irrigation experiments in the LIS configuration file.

Irrigation type	Flood irrigation	Sprinkler irrigation
• 0 for non-irrigation experiment • 1 for flood irrigation • 2 for drip irrigation • 3 for sprinkler irrigation	• Irrigation trigger coefficient : 0.25 (default) • Irrigation time in local time • Irrigation frequency: 0 (do not use) or irrigation intervals in days	• Irrigation trigger coefficient : 0.1 (default) • Irrigation off coefficient : 0.2 (default) • Average sprinkler application rate: 5.0 mm h-1 (default)

3.2. Land surface states and fluxes

3.2.1. Murray-Darling basin

Major irrigation districts in the Murray-Darling basin are presented in Fig. 5. As illustrated, the simulated irrigation regions (Fig. 5 (b)) were well matched with the observed irrigation regions (Fig. 5 (a)). Initially, the USGS landcover map did not identify the irrigation districts in the basin very well (data not shown). Locally

surveyed irrigation maps were combined with the USGS landcover map to improve the irrigation coverage in the basin. These surveyed maps may lead to the identification of further irrigation regions in the basin.

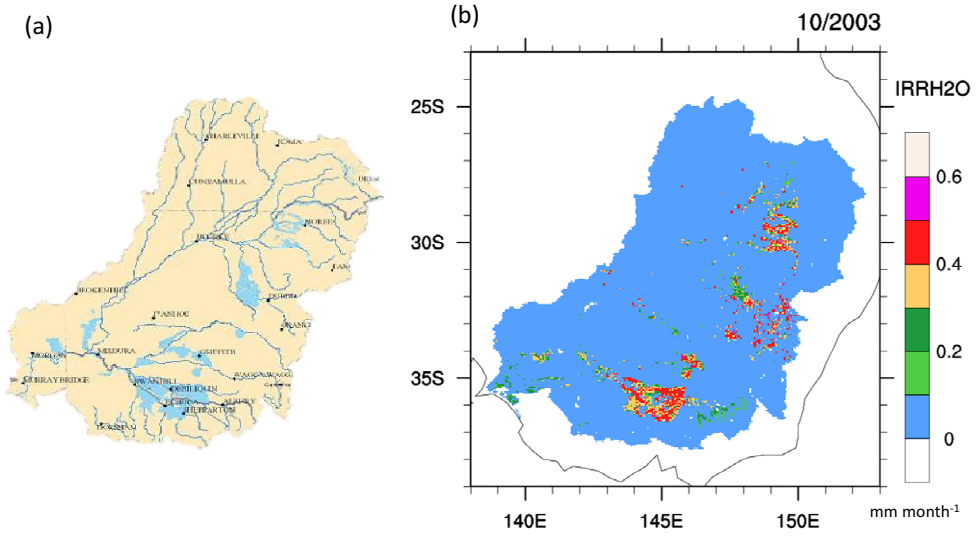

Figure 5 Major irrigation districts in the Murray-Darling basin: (a) observed (adapted from Murray-Darling Basin Commission, 2005) and (b) simulated irrigation districts. IRRH2O: irrigation amount in mm month^{-1}.

Fig. 6 describes the monthly irrigation amount in GL (gigaliters) in the Murray-Darling basin. Peak irrigation occurred in October 2002 and tended to decrease thereafter. The total amount of irrigation by IR3 (sprinkler irrigation) was the largest, followed by IR1 (flood irrigation). The monthly irrigation amount of IR1 varied the most, ranging from 70 to 730 GL, while the range in the amount of irrigation by IR2 (drip irrigation) was the smallest. Irrigation amounts between July 2002 and June 2003 were simulated as 3622, 837, and 7648 GL for IR1, IR2, and IR3, respectively. The total irrigation water in Australia in 2002/3 was 10,403 GL (ABS, 2006). It was estimated that 75% of this amount (i.e., approximately 7800 GL) was used in the Murray-Darling basin in 2002/3. IR3 was simulated to be closest to the estimated amount of irrigation in the basin.

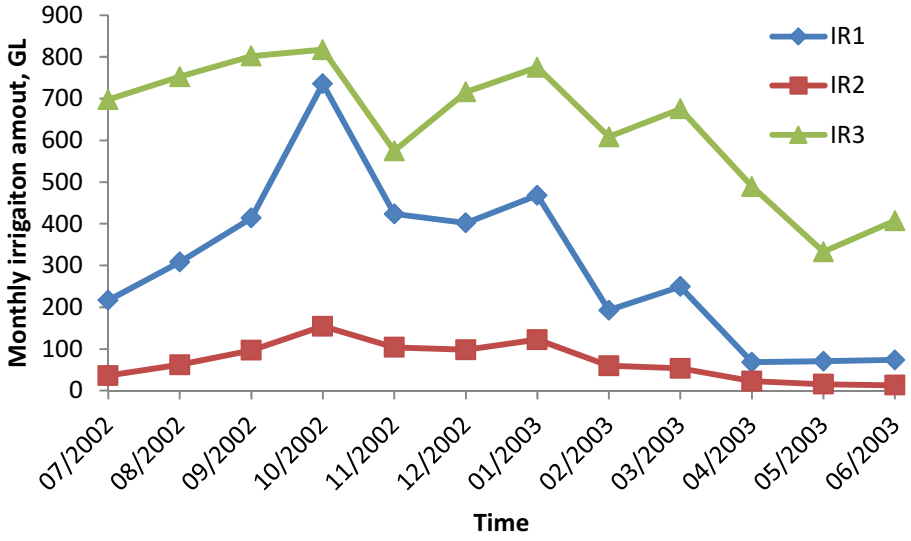

Figure 6 Simulated monthly irrigation amount within the Murray-Darling basin. IR1: flood irrigation, IR2: drip irrigation, and IR3: sprinkler irrigation.

Monthly mean precipitation, irrigation amount, surface runoff, evapotranspiration, and soil moisture are presented in Fig. 7. Soil moisture was calculated as a mean of the first three depths (between the surface and 0.6 m deep). As shown in Fig. 7 (a), monthly mean precipitation in January 2003 was smallest, while that in February 2003 was largest. Peak irrigation amount of IR1 and IR3 occurred in October 2002 and February 2003, respectively (Fig. 7 (b)). Monthly mean evapotranspiration and soil moisture (Fig. 7 (d) and (e)) were increased in the three irrigation experiments (i.e., IR1, IR2, and IR3). However, a significant increase in monthly mean surface runoff was seen in IR3 only (Fig. 7 (c)). This result implies that surface runoff is more sensitive to precipitation than to irrigation.

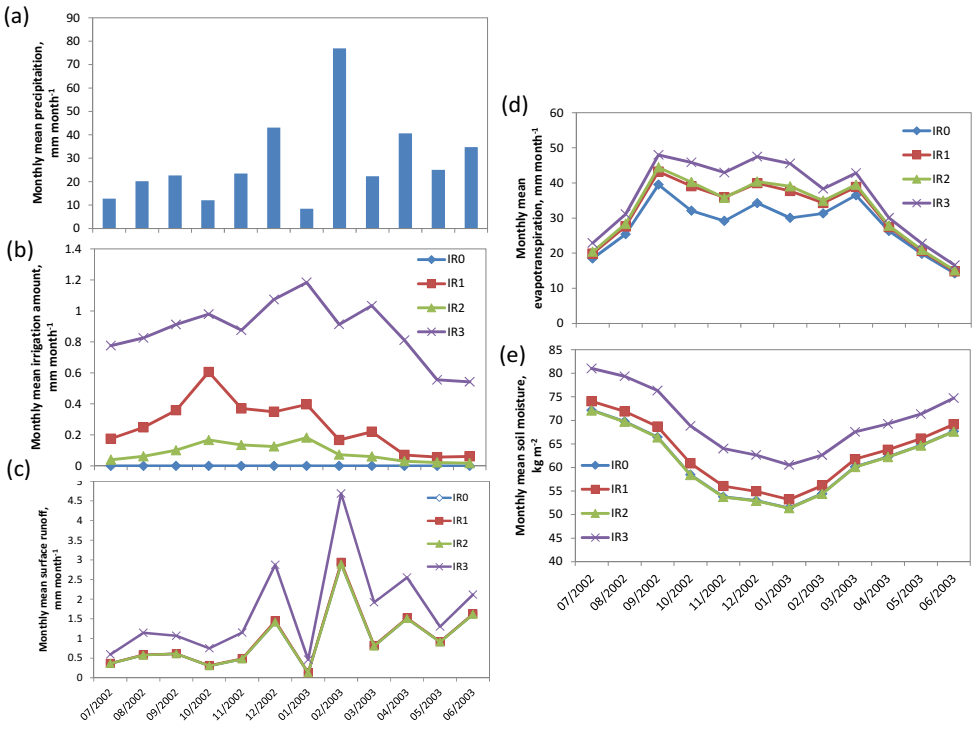

Figure 7 Monthly mean (a) precipitation, (b) simulated irrigation amount, (c) simulated surface runoff, (d) simulated evapotranspiration, and (e) simulated soil moisture. Soil moisture is the depth-averaged value calculated between the surface and 0.6m deep. IR0: non-irrigation, IR1: flood irrigation, IR2: drip irrigation, and IR3: sprinklerirrigation.

Fig. 8 presents the mean energy budget components and water budget components averaged over the entire Murray-Darling basin and one entire year (July 2002 to June 2003). As shown in Fig. 8 (a), irrigation showed a tendency to increase the latent heat flux (QLE) and ground heat flux (QG), while it resulted in a decrease of the sensible heat flux (QH). Changes in the energy budget components were largest in the IR3 experiment. For example, QLE was increased by 7.7 Wm^{-2} (29%) in the IR3 experiment compared to the IR0 experiment. Ground heat flux (QG) slightly increased by 1% in the IR3 experiment, while sensible heat flux (QH) decreased by 7% (6.4 Wm^{-2}). For the IR3 experiment, irrigation increased evapotranspiration, surface runoff, and soil moisture by 29, 78, and 14%, respectively (Fig. 8 (b)). These results are in very good agreement with those by Ozdogan *et al.* (2010), who found that irrigation led to changes in water and energy budget components.

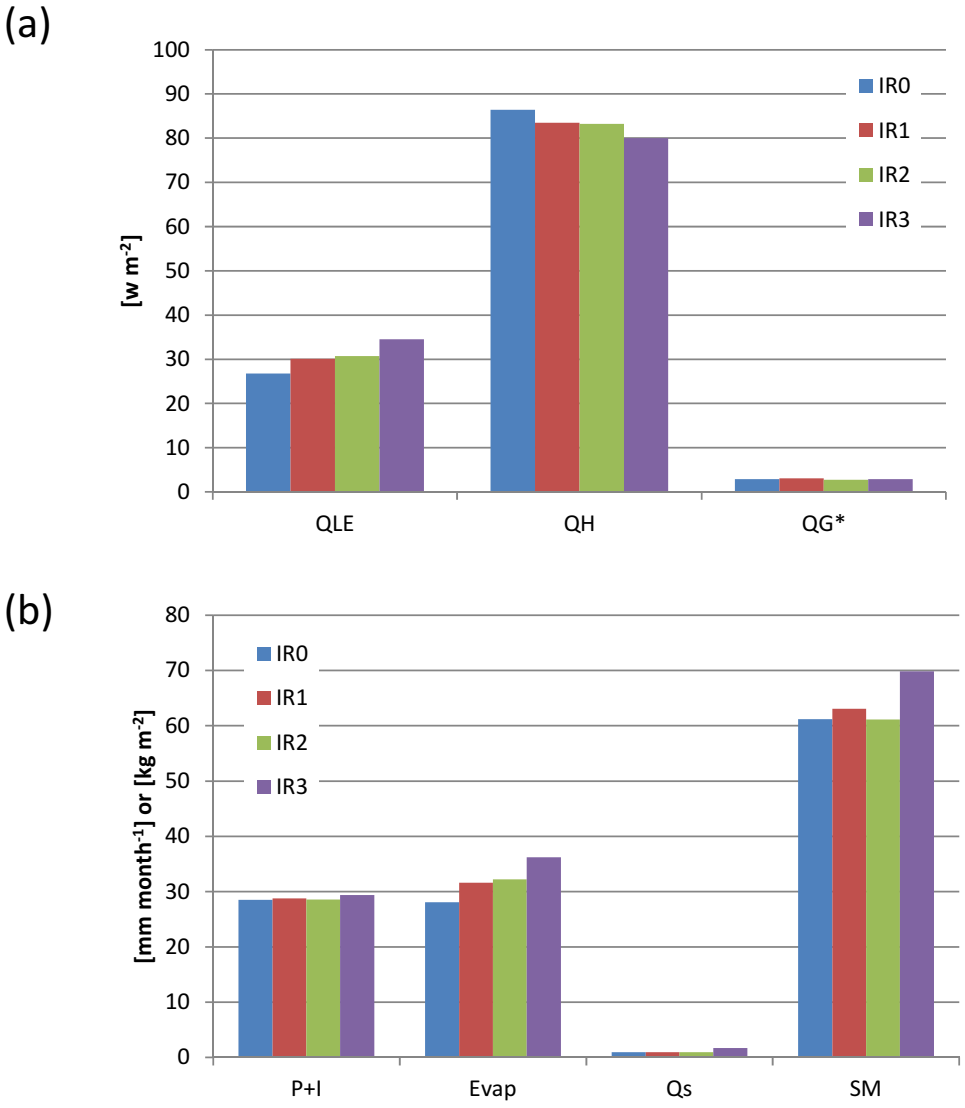

Figure 8 Mean (a) energy budget components and (b) water budget components averaged over the entire Murray-Darling basin and an entire year (July 2002 to June 2003). QLE: Sensible heat flux, Wm^{-2} QH: Sensible heat flux, Wm^{-2}, QG*: Ground heat flux, 0.1 Wm^{-2}, IR0: non-irrigation, IR1: flood irrigation, IR2: drip irrigation, IR3: sprinklerirrigation, P+I: precipitation + irrigation amount, mm $month^{-1}$, ET: evapotranspiration, mm $month^{-1}$, Qs: surface runoff, mm $month^{-1}$, and SM: depth-averaged soil moisture between the surface and 0.6 m depth.

3.2.2. East Asia and the Korean Peninsula

As shown in Fig. 9, the model simulated irrigation water to be greatest in the region from 105° to 120°E and from 25° to 40°N, and that irrigation peaks in May. Spring wheat is mainly cultivated in this region and its growing season is in May. However, the model failed to adequately capture agricultural fields in Korea and Japan. It is likely that this limitation resulted from the coarse spatial resolution of 25km used in the model simulation. The limited computational resources constrained this spatial resolution. The loss of information as a result of this limitation suggests that land surface states and fluxes should be investigated on a country scale with a spatial resolution of at least 1 km. Furthermore, since the USGS landcover map was used to identify irrigated areas for this study, an investigation is suggested, into whether the USGS landcover map accurately represents the actual irrigated areas in this region.

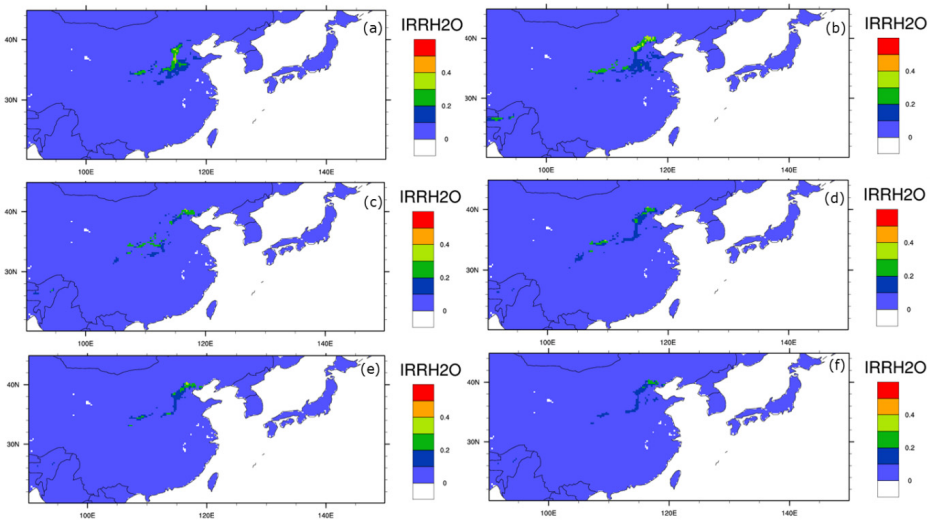

Figure 9 Monthly averaged irrigation amount (IRRH2O) in mm day^{-1} from 2001 to 2010: (a) April, (b) May, (c) June, (d) July, (e) August, and (f) September.

As shown in Fig. 9, the irrigation water was applied to an area from 30° to 40°N and from 110°to 120°E. The water budget in the area was investigated and is presented in Fig. 10. Mean monthly rainfall during the growing season ranged

from 4.9 × 10^{14} to 1.8 × 10^{15}kg month^{-1}. Over this period, mean monthly evapotranspiration in the area varied between 5.8 × 10^{14} and 1.1 × 10^{15}kg month^{-1} and mean monthly irrigated water ranged from 5.1 × 10^{12} and 1.2 × 10^{13}kg month^{-1}. More irrigation water was applied in spring (April and May) when less precipitation occurred, while peak precipitation and evapotranspiration occurred in July.

The flood irrigation scheme, which is switched on when the soil moisture in the first soil layer falls below the threshold value (25% above wilting point for this study), has not been properly evaluated against the observed irrigation practices in this region. However, the proposed irrigation scheme can be used to qualitatively investigate the impacts of irrigation schemes on the components of the hydrologic cycle, since the simulation results showed that the irrigation amounts in the region well matched the growing seasons.

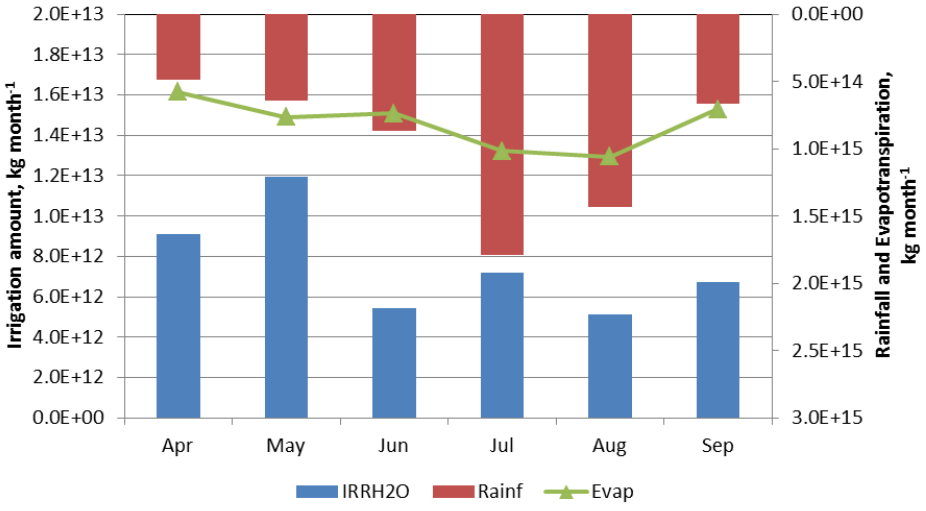

Figure 10 Mean monthly irrigation amount, rainfall, and evapotranspiration in an area inside the study region (from 30° to 40°N and from 110°to 120°E). IRRH2O, Rainf, and Evap represent irrigation amount, rainfall, and evapotranspiration, respectively.

Mean monthly differences in evapotranspiration between the flood irrigation and non-irrigation schemes are presented in Fig. 11 as a series of monthly maps. Peak evapotranspiration in the region generally occurred in May. With the flood irrigation

scheme, evapotranspiration showed a tendency to increase over the growing season. This tendency is in substantial agreement with the conclusions of Ozdogan *et al.* (2010). The largest difference in evapotranspiration in a grid cell between the flood irrigation- and the non-irrigation-simulations was approximately 130 mm month^{-1}. This difference in a single grid cell is similar to that found by Ozdogan *et al.* (2010), who reported that the largest difference in an extreme case was around 170 mm month^{-1}.

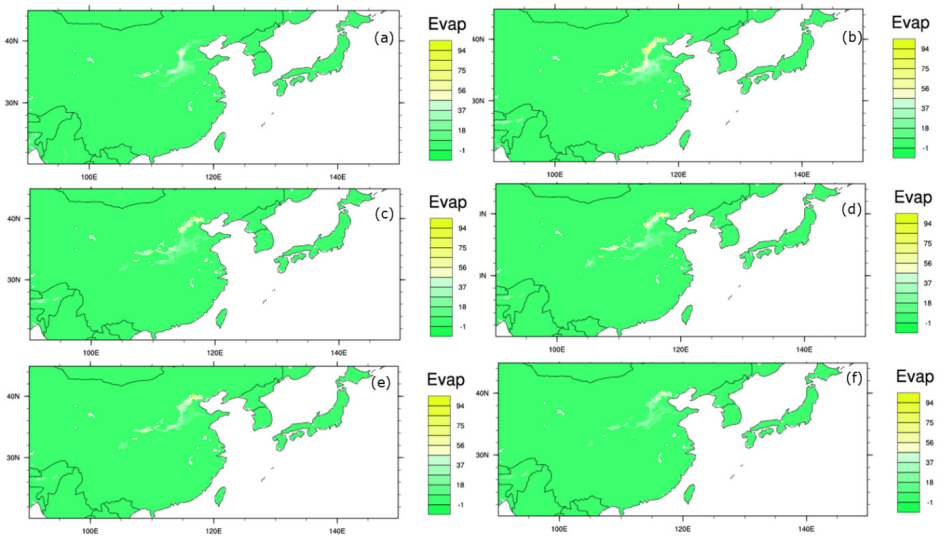

Figure 11 Monthly average of evapotranspiration (Evap) difference between flood irrigation and non-irrigation in kg m^{-2} month^{-1} from 2001 to 2010: (a) April, (b) May, (c) June, (d) July, (e) August, and (f) September.

Simulated results of the energy fluxes over the growing season are presented in Figs. 12 to 14. Peak changes in the energy fluxes generally occurred in May. The flood irrigation scheme increased latent heat flux (QLE), decreased sensible heat flux (QH), and slightly increased ground heat flux (QG). The largest changes in a single grid cell were approximately 120, -110, and 4 Wm^{-2} for QLE, QH, and QG, respectively. These changes are similar in tendency to those reported by Ozdogan *et al.* (2010) and in good agreement with those by Adegoke *et al.* (2003). The latter authors found that the differences between results from irrigated and non-irrigated experiments in central Nebraska (U.S.A.) were significant. However, unlike latent heat flux and sensible heat flux, ground heat flux tended to slightly decrease over the irrigated

areas in August and September. This inconsistency suggests that a further study on the energy fluxes in the irrigated areas over the growing season will be necessary.

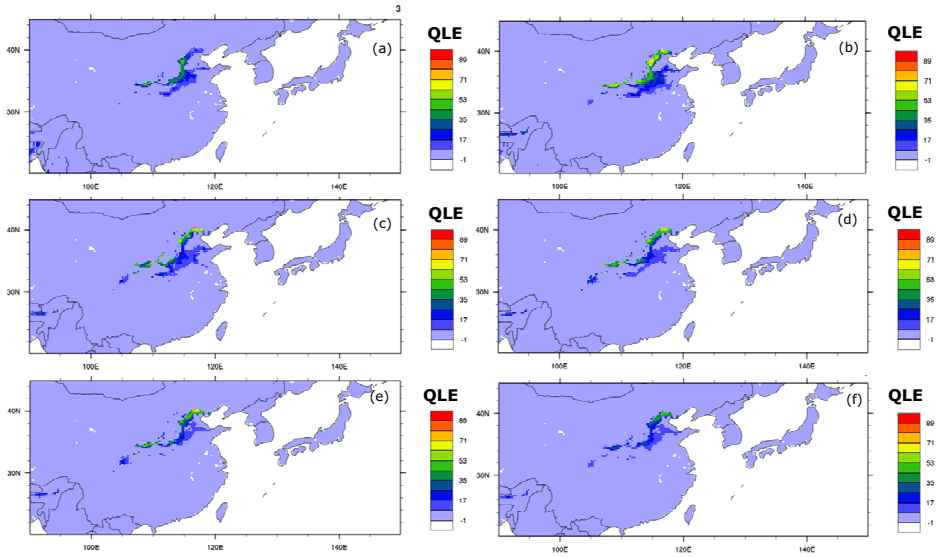

Figure 12 Monthly average difference in latent heat flux (QLE) between flood irrigation and non-irrigation situations in Wm^{-2} from 2001 to 2010: (a) April, (b) May, (c) June, (d) July, (e) August, and (f) September.

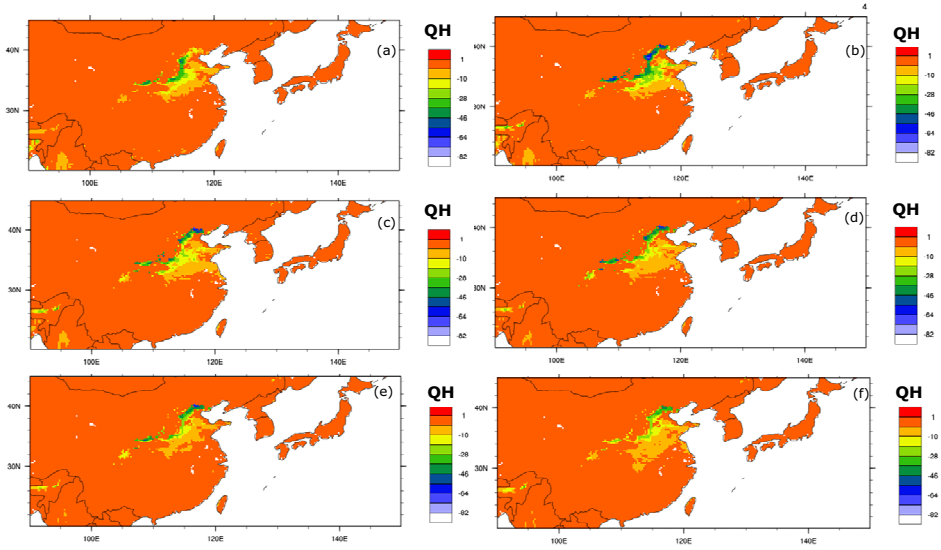

Figure 13 Monthly average difference in sensible heat flux (QH) between flood irrigation and non-irrigation situations in Wm^{-2} from 2001 to 2010: (a) April, (b) May, (c) June, (d) July, (e) August, and (f) September.

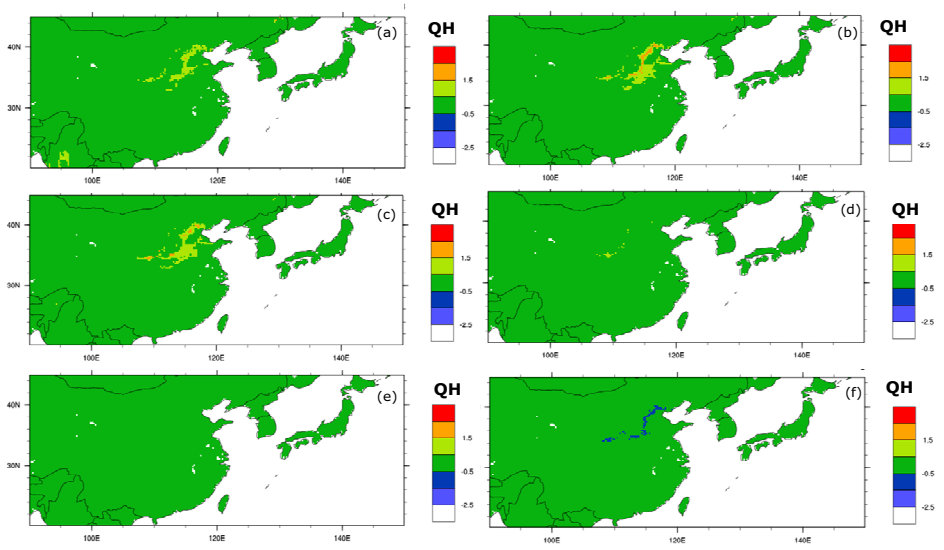

Figure 14 Monthly average difference in ground heat flux (QG) between flood irrigation and non-irrigation situations in Wm^{-2} from 2001 to 2010: (a) April, (b) May, (c) June, (d) July, (e) August, and (f) September.

In general, irrigation raises the soil moisture. Mean monthly differences in soil moisture at each layer (up to 1.0m deep) are presented in Figs. 15 to 18. Peak changes in soil moisture in each layer generally occurred in May. While the changes in soil moisture up to the third layer (0.6m deep) showed a tendency to increase over the irrigated areas and during the growing season, those in the fourth layer (0.6 to 1.0m deep) did not show any apparent tendency over the irrigated areas or during the growing season. The flood irrigation scheme will saturate the first soil layer (between the surface to 0.1m deep) once it is triggered. These findings imply this additional water from the flood irrigation contributes to the increases in moisture in the first three soil layers from the surface (i.e., between the surface and 0.6m deep). However, unlike the increases up to the first three layers, the additional water does not seem to directly affect the fourth soil layer because irrigated water that is applied only to the first soil layer may not be close enough to penetrate to the fourth layer.

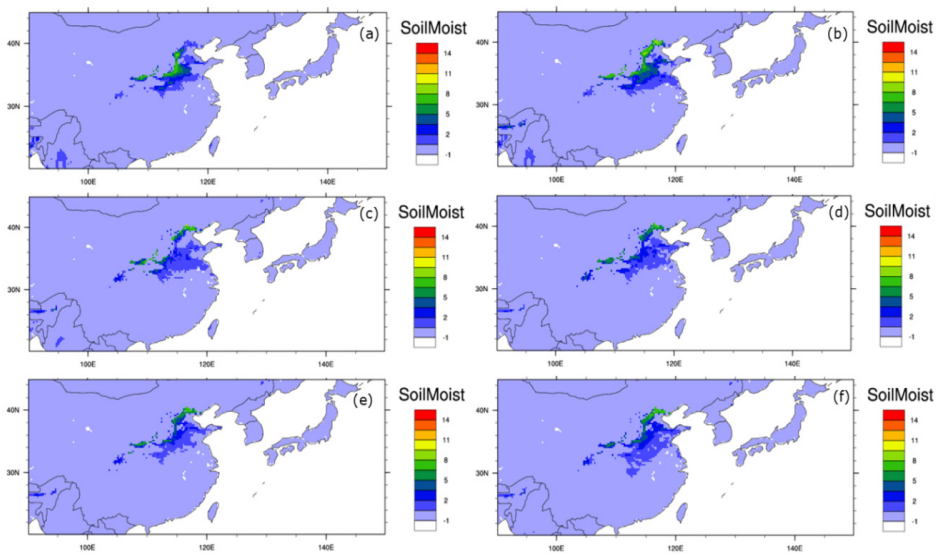

Figure 15 Monthly average difference in soil moisture (SoilMoist) at the first layer (between the surface and 0.1m depth) between flood irrigation and non-irrigation in kgm^{-2} from 2001 to 2010: (a) April, (b) May, (c) June, (d) July, (e) August, and (f) September.

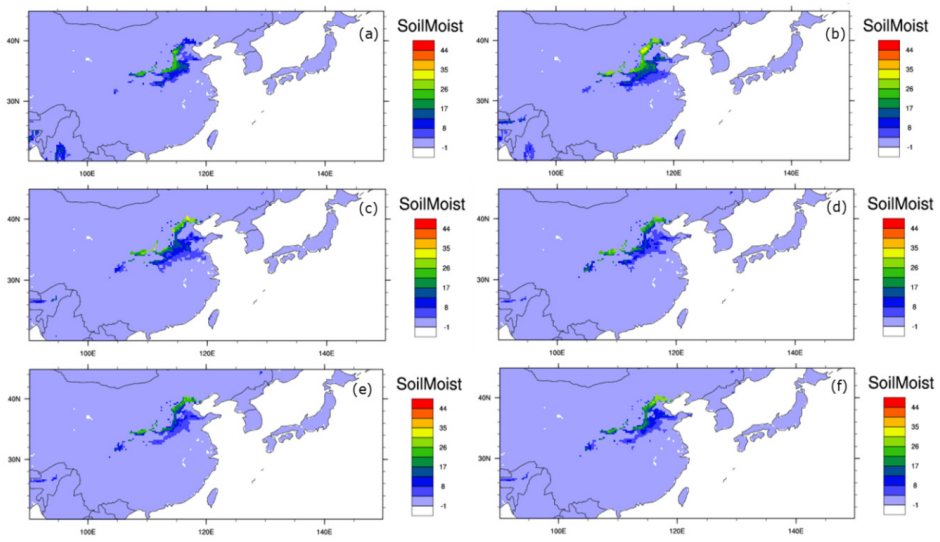

Figure 16 Monthly average difference in soil moisture (SoilMoist) in the second layer (between 0.1 and 0.3 m depth) between flood irrigation and non-irrigation in kgm^{-2} from 2001 to 2010: (a) April, (b) May, (c) June, (d) July, (e) August, and (f) September.

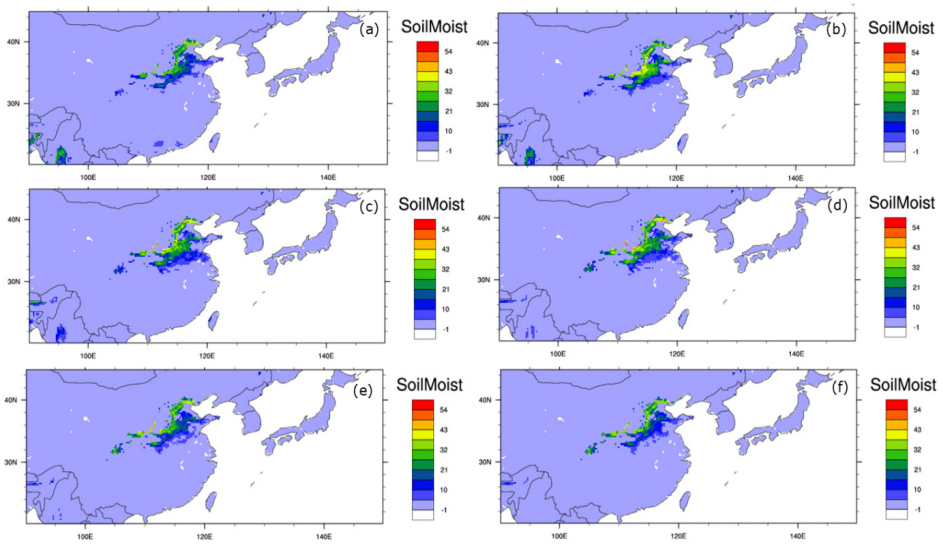

Figure 17 Monthly average difference in soil moisture (SoilMoist) in the third layer (between 0.3 and 0.6 m depth) between flood irrigation and non-irrigation in kgm^{-2} from 2001 to 2010: (a) April, (b) May, (c) June, (d) July, (e) August, and (f) September.

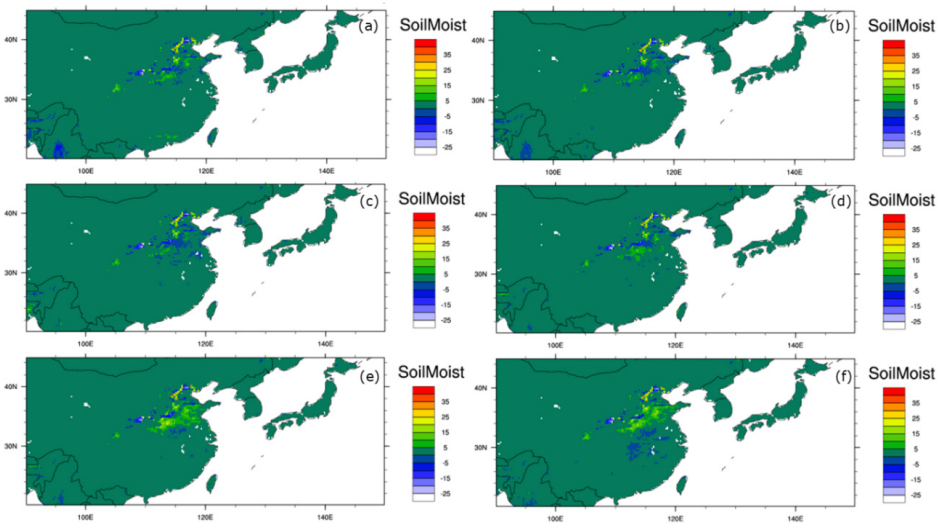

Figure 18 Monthly average difference in soil moisture (SoilMoist) in the fourth layer (between 0.6 and 1.0 m depth) between flood irrigation and non-irrigation in kgm^{-2} from 2001 to 2010: (a) April, (b) May, (c) June, (d) July, (e) August, and (f) September.

4. SUMMARY and CONCLUSIONS

The three irrigation schemes, flood irrigation, drip irrigation, and sprinkler irrigation, were incorporated into the Noah-LSM model in the LIS. The tool was applied to the Murray-Darling basin and to East Asia and the Korean Peninsula. Although these three irrigation schemes were applied to the Murray-Darling basin, predominant irrigation practices in East Asia and the Korean Peninsula, led to the use of only a traditional flood irrigation scheme in this region. However, this scheme might not be adequate to represent rice-paddy ecosystems with flooding conditions. It is therefore recommended that this limitation be addressed in future studies.

Crop growing seasons were determined using the Moderate Resolution Imaging Spectrometer (MODIS) vegetation index for a global experiment. The Noah-LSM was spun up using GDAS and TRMM meteorological forcing data, and investigated the hydrologic flux estimates in the East Asian region for 10 years (2001 to 2010). In the two study regions, evapotranspiration under the flood irrigation scheme showed a tendency to increase over the growing season. The scheme also increased soil moisture in the first three soil layers (from the surface to 0.6 m deep), while there was no apparent tendency in the fourth soil layer (from 0.6 to 1.0 m deep). The irrigation schemes increased latent heat flux (QLE) and ground heat flux (QG), but decreased sensible heat flux (QH). These results are in substantial agreement with those of previous studies.

It is therefore concluded that the proposed irrigation scheme can be used to qualitatively investigate impacts on land surface states and fluxes in East Asia and the Korean Peninsula.

REFERENCES

Adegoke, J.O., R.A. Pielke, J. Eastman, R. Mhamood, and K.G. Hubbard. 2003. Impact of irrigation on midsummer surface fluxes and temperatures under dry synoptic conditions: A regional atmospheric model study of the U.S. high plains. Monthly Weather Review, 131, 556-564.

Abreu, P., M. Aglietta, M. Ahlers, E.J. Ahn, I.FM. Albuquerque, D. Allard, ··· M. Ziolkowski. 2012. Description of atmospheric conditions at the Pierre Auger Observatory using the Global Data Assimilation System (GDAS). Astroparticle Physics, 35, 591-607.

Australian Bureau of Statistics (ABS). 2006. Water use on Australian Farms 2004-05. ABS Catalogue No. 4618.0.

Australian Natural Resources Atlas (ANRA). n.d. retrieved from http://www.anra.gov.au/topics/irrigation/images/mdb_case/mdb_ag_stats.html#overview

Ben-Gai, T., A. Bitan, M. Manes, and P. Alpert. 2001. Climatic variations in the moisture and instability patterns of the atmospheric boundary layer on the East Mediterranean coastal plain of Israel. Boundary-Layer Meteorology, 100, 363-371.

Betts, A., F. Chen, K. Mitchell, and Z. Janjic. 1997. Assessment of the land surface and boundary layer models in two operational versions of the NCEP Eta model using FIFE data. Monthly Weather Review, 125, 2896-2916.

Bonan, G.B. 1997. Effects of Land Use on the Climate of the United States. Climatic Change, 37, 449-486.

Bonan, G.B. 2001. Observational evidence for reduction of daily maximum temperature by croplands in the Midwest United States. Journal of Climate, 14, 2430-2442.

Chase, T.N., R.A. Pielke Sr., T.G.F. Kittel, R. Nemani, and S.W. Running. 2000. Simulated impacts of historical land cover change son global climate in northern winter. Climate Dynamics, 16, 93-105.

Ek, M.B., K.E. Mitchell, Y. Lin, E. Rogers, P. Grunmann, V. Koren, G. Gayno, and J.D. Tarpley. 2003. Implementation of Noah land surface model advances in the National Centers for Environmental Prediction operational mesoscale Eta model. Journal of Geophysical Research, 108, 8851

Evans, J.P. and B.F. Zaitchik. 2008. Modeling the large-scale water balance impact of different irrigation systems. Water Resources Research, 44, W08448, doi:10.1029/2007WR006671.

FAO. 2007. Water at a Glance: The relationship between water, agriculture, food security and poverty. Retrieved from http://www.fao.org/nr/water/docs/waterataglance.pdf

Gesch, D.B., K.L. Verdin, and S.K. Greenlee. 1999. New land surface digital elevation model covers the Earth. Eos, Transactions, American Geophysical Union, 80, 69-70.

Goddard Space Flight Center, National Aeronautics and Space Administration. 2010a. LIS Developer's Guide. Version 6.0. Greenbelt, MD, USA.

Goddard Space Flight Center, National Aeronautics and Space Administration. 2010b. LIS User's Guide. Revision 6.1. Greenbelt, MD, USA.

Haddenland, I., D.P. Lettenmaier, and T. Skaugen. 2006. Effects of irrigation on the water and energy balances of the Colorado and Mekong river basins. Journal of Hydrology, 324, 210-223.

Huffman, G.J., R.F. Adler, D.T. Bolvin, G. Gu, E. J. Nelkin, K.P. Bowman, Y. Hong, E.F. Stocker, and D.B. Wolff. 2007. The TRMM Multisatellite Precipitation Analysis (TMPA): Quasi-global, multiyear,

combined-sensor precipitation estimates at fine scales. Journal of Hydrometeorology, 8, 38-55.

Koren, V., J. Schaake, K. Mitchell, Q.-Y. Duan, F. Chen, and J.M. Baker. 1999. A parameterization of snowpack and frozen ground intended for NCEP weather and climate models. Journal of Geophysical Research, 104, 19 569-19 585.

Kumar, S.V., C.D. Peters-Lidard, Y. Tian, P.R. Houser, J. Geiger, S. Olden, L. Lighty, J.L. Eastman, B. Doty, P. Dirmeyer, J. Adams, K. Mitchell, E.F. Wood, J. Sheffield. 2006. Land information system: An interoperable framework for high resolution land surface modeling. Environmental Modelling and Software, 21, 1402-1415.

Lamaddalena, N., U. Fratino, and A Daccache. 2007. On-farm sprinkler irrigation performance as affected by the distribution system, Biosystems Engineering, 96, No 1, 99–109.

Lobell, D.B., and C. Bonfils. 2008. The effect of irrigation on regional temperatures: A spatial and temporal analysis of trends in California, 1934-2002. Journal of Climate, 21, 2063-2071.

Lobell, D.B., C. Bonfils, and J.M. Faures. 2008. The role of irrigation expansion in past and future temperature trends. Earth interactions, 12, 1-11.

Moore, N., and S. Rojstaczer. 2002. Irrigation's influence on precipitation: Texas High Plains, U.S.A. Geophysical Research Letters, 29, 1755.

Murray-Darling Basin Commission. 2005. eResource Book. Retrieved from http://www2.mdbc.gov.au/subs/eResource_book.

Murray-Darling Basin Authority. n.d. Retrieved from http://www.mdba.gov.au/annualreports/2008-09/role.html.

Ozdogan, M., G.D. Salvucci, and B.C. Anderson. 2006. Examination of the Bouchet-Morton complementary relationship using a meso-scale climate model and observations under a progressive irrigation scenario. Journal of Hydrometeorology, 7, 235-251.

Ozdogan, M., M. Rodell, H.K. Beaudoing, D.L. Toll. 2010. Simulating the effects of irrigation over the United States in a land surface model based on satellite-derived agricultural data. Journal of Hydrometerology, 11, 171-184.

Parrish, D. F., and J. C. Derber, 1992: The National Meteorological Center's spectral statistical interpolation analysis system. Monthly Weather Review, 120, 1747-1763.

Reynolds, C.A., T.J. Jackson, and W.J. Rawls. 2000. Estimating soil water-holing capacities by linking the Food and Agriculture Organization Soil Map of the World with global pedon databases and continuous pedotransfer functions. Water Resources Research, 36, 3653-3662.

Sorooshian, S., J. Li, K.-L. Hsu, and X. Gao. 2012. Influence of irrigation schemes used in regional climate models oon evapotranspiration estimation: Results and comparative studies from California's Central Valley agricultural regions. Journal of Geophysical Research, 117, D06107, doi:10.1029/2011JD016978.

Takata, K., Emori, S., and Watanabe, T. 2003. Development of the minimal advanced treatments of surface interaction and runoff. Global and Planetary Change, 38, 209–222.

U.S. Geological Survey. (n.d.). global land cover characteristics data base version 2.0. Retrieved from http://edc2.usgs.gov/glcc/globdoc2_0.php#app3.

APCC TECHNICAL REPORT 2012-02

- Evaluation of Water Balance on a Regional Scale
- Analysis of Climatic Trends over South Asia
- Study of Aerosol Effect on Accelerated Snow Melting
- Aerosol Variability on Global and Regional Scales
- Evaluation of a Distributed Hydrologic Model

APEC Climate Center

12, Centum 7-ro, Haeundae-gu, Busan 612-020,
Republic of Korea
Tel: +82-51-745-3900 Fax: +82-51-745-3949
www.apcc21.org

비매품
9 788997 333370
ISBN 978-89-97333-37-0
ISBN 978-89-97333-35-6 (세트)